

**FULL ARTICLE**

# Guided filter based image enhancement for focal error compensation in low cost automated histopathology microscopic system

Navchetan Awasthi<sup>1,2,3</sup> | Prateek Katare<sup>4</sup> | Sai Siva Gorthi<sup>4</sup> |  
Phaneendra K. Yalavarthy<sup>1\*</sup> 

<sup>1</sup>Department of Computational and Data Sciences, Indian Institute of Science, Bangalore, India

<sup>2</sup>Cardiovascular Research Centre, Massachusetts General Hospital, Boston, Massachusetts

<sup>3</sup>Harvard University, Cambridge, Massachusetts

<sup>4</sup>Department of Instrumentation and Applied Physics, Indian Institute of Science, Bangalore, India

**\*Correspondence**

Phaneendra K. Yalavarthy, Department of Computational and Data Sciences (CDS), Indian Institute of Science, Bangalore 560012, India.

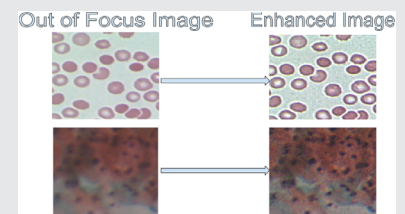
Email: yalavarthy@iisc.ac.in

**Funding information**

IFTAS-CDS Collaborative Laboratory of Data Science and Engineering; DST-ICPS, Grant/Award Number: T-851

**Abstract**

Low-cost automated histopathology microscopy systems usually suffer from optical imperfections, producing images that are slightly Out of Focus (OoF). In this work, a guided filter (GF) based image preprocessing is proposed for compensating focal errors and its efficacy is demonstrated on images of healthy and malaria infected red blood cells (h-RBCs and i-RBCs), and PAP smears. Since contrast enhancement has been widely used as an image preprocessing step for the analysis of histopathology images, a systematic comparison is made with six such prominently used methods, namely Contrast Limited Adaptive Histogram Equalization (CLAHE), RIQMC-based optimal histogram matching (ROHIM), modified  $L_0$ , Morphological Varying(MV)-Bitonic filter, unsharp mask filter and joint bilateral filter. The images enhanced using GF approach lead to better segmentation accuracy (upto 50% improvement over native images) and visual quality compared to other approaches, without any change in the color tones. Thus, the proposed GF approach is a viable solution for rectifying the OoF microscopy images without the loss of the valuable diagnostic information presented by the color tone.

**KEYWORDS**

blood or tissue constituent monitoring, cell analysis, clinical applications, medical optics instrumentation, microscopy, systems

**1 | INTRODUCTION**

Access to timely and affordable diagnosis of medical disorders is a prerequisite for quality healthcare. However, such diagnostic facilities are often unavailable to more than a billion low-income residents of developing countries. For this reason, the World Health Organization (WHO) has prioritized development of methods that can

enable affordable and rapid diagnostic procedures. A promising way of achieving this goal is automation of sample and data processing. One routinely conducted diagnostic examination that could vastly benefit from this is the microscopic observation of slide smears [1]. A typical smear of a biological specimen, such as human blood or cervical cells, requires a trained technician to observe the slide under a microscope at multiple fields of view

(FoV) for qualitative and quantitative assessment. For instance, WHO recommends that a blood smear should be observed at 800 different FoV before a negative diagnosis of Malaria is established [2]. Such a laborious process is inherently time consuming as well as prone to human errors. This problem can be alleviated by automated microscopy image acquisition and image analysis methods. Systems that can acquire a complete microscopy image of a slide smear without any human involvement would vastly reduce the workload of the pathologist and thus improve the diagnostic accuracy too. Such systems, termed as whole slide imaging (WSI) systems, form a crucial part of the paradigm of digital pathology [3–5]. These systems can be subsequently coupled with automated image analysis to produce standalone diagnostic devices, which are useful for point-of-care diagnostics.

Unfortunately, the current available commercial products for this purpose are not aimed at low-resource settings and are typically priced above US \$ 100 000 [6]. Some research groups have attempted to develop more affordable alternatives by using low-cost components and fabrication methods. These provide acceptable quality of imaging while excluding all frills to arrive at a substantial cost reduction [6]. However, imperfections in their linear translation mechanisms lead to images that are Out of Focus (OoF), requiring a focal stack to be acquired at each FoV for selection of one best focused image. This reduces the throughput of the system, rendering them useful only for research purposes.

Consider, for instance, the standard microscope glass slide, of specimen area 50 mm x 25 mm, used for preparing smears. Scanning an entire slide of this dimension will result in a set of about 14 000 microscopy images, using a typical low-cost camera with a 36.8 mm<sup>2</sup> sensor area at a modest magnification of  $\times 20$ . At a scan rate of 30 frames per second (FPS), obtaining the WSI would be accomplished in about 8 min for an optically perfect system. But, for an imperfect system, acquisition of a focal stack consisting of 10 images or so at each FoV will be necessary for selecting the image with best focus. As a result, the time required for a WSI will be more than 80 min along with added computational complexity for selection of best focused image. This defeats the purpose of rapid and affordable diagnostics by decreasing the throughput of the system.

Importantly, the optical imperfections may not be a matter of concern if native images could be enhanced to become suitable for further automated image analysis and hence arrival at a viable diagnostic result. Such an enhancement method will aim at sharpening features in the image so as to mimic better focus and thus allow further image processing to achieve accurate results. Image enhancement has been a topic of wide interest and the

available literature in this regard is either centered around enhancing the depth of focus of the imaging system [7] or fusing a stack of images with different sections in focus to achieve a single well-focused image [8, 9].

In this work, a guided filter (GF) [10, 11] based approach is introduced to enhance the OoF images, leading to significantly increased visual quality. This improvement is demonstrated through results of further image processing via segmentation (an essential step in most bio-medical image processing pipelines). Six other methods for image enhancement are also compared with the proposed GF technique. These are Contrast Limited Adaptive Histogram Equalization (CLAHE) [12] based on histogram equalization, RIQMC-based optimal histogram matching (ROHIM) [13], modified  $L_0$  [14], Morphological Varying(MV)-Bitonic based method [15], unsharp mask filtering [16], and joint bilateral filter [17]. The CLAHE is a standard local contrast enhancement technique which enhances the minute details of the image effectively and hence was a natural choice for comparison with GF method. Since it over-enhances the image, ROHIM was chosen as it is a more refined method. However, it was found to alter the color tone of the image and thus modified  $L_0$ , another well-known enhancement method was used. Another technique MV-Bitonic filtering was used to enhance the image quality, which gave a slightly visually improved output without improvement in the segmentation results. Another important class of filtering techniques used here is unsharp masking, used for enhancement of blurred images. This class includes the widely used bilateral filter, which is an explicit weighted average filter. It averages neighboring pixels, weighted by Gaussian of intensity and spatial distance to get the filtering output. It smoothens the image while maintaining the edges and has been widely used for noise reduction and image enhancement [18]. It has been already shown that GF performs better than the bilateral filter [10, 11], so a joint bilateral filter has instead been utilized in this work for comparison [17]. However, for completeness, comparisons with a simple unsharp mask have been included. Comparison results with these six methods suggest that GF based approach is more suitable for improving accuracy of automated algorithms that are typically deployed for segmentation. It does not require any additional information, other than the source image, and uses the implicit regularization scheme to enhance the features with an added advantage of being computationally efficient.

The GF based enhancement was shown to make even low quality OoF images suitable for clinical assessment. Moreover, the enhancement in the visual quality of microscopy images is helpful for inspection by trained clinicians. Their feedback would be a necessary step in

developing and improving the accuracy of machine learning based image processing algorithms. This would complete the development loop toward an automated, affordable diagnostic device. Thus, this work demonstrates an affordable solution for solving an universal healthcare puzzle and might greatly help in lowering the diagnostic costs by providing accurate results even with sub-optimal equipment.

## 2 | MATERIALS AND METHODS

### 2.1 | Setup for acquiring microscopy images

The microscopy images used in this work were acquired from a low-cost automated microscopy setup as detailed in Section 2 of this work. A low-cost microscopy setup was built with a choice of a  $\times 20$  or a  $\times 40$  PLAN objective lens (Lawrence & Mayo) to magnify the biological sample under illumination with a 3 W white LED, along with suitable optics. The sample was imaged with a 1.3 Megapixel CMOS camera (Ximea GmbH) delivering raw pixel data to a computing unit, via a USB-3 connection, at a frame rate of over 20 FPS. A digital logic board was used to control the actuation along all the three axes, providing control over the area being observed as well as the focus on the specimen. All components were chosen with the objective of keeping the cost and footprint of the device as low as possible. A close-up view of the imaging section of the setup can be seen in Figure 1A. Focal stacks were acquired at multiple FoVs to retrieve the best focused images as well as OoF images for the purpose of

experiments performed here. The typical process involved in the focal stack acquisition is given in Figure 1B. The acquired images undergo an image enhancement step before any processing to enrich the diagnostic information present in the microscopy images. The six standard image enhancement methods and the one proposed in this work are detailed below.

### 2.2 | Contrast limited adaptive histogram equalization based enhancement

It is a standard local contrast enhancement technique which enhances the minute details of the image effectively. The main steps of contrast limited adaptive histogram equalization (CLAHE) include [12] -

- Partitioning of the image into patches that are non-overlapping and continuous.
- Clipping the histogram for each tile above a threshold level and distributing the clipped pixels to all gray levels.
- Applying histogram equalization on each tile separately.
- Interpolation of the mapping between separate tiles. In general, the intensity mapping of four neighboring tiles is used for interpolation to get the resultant mapping at each pixel.

The disadvantages of CLAHE based enhancement are excessive enhancement leading to image distortion [12], significant computation time required by the histogram equalization (HE) and the noise also being enhanced

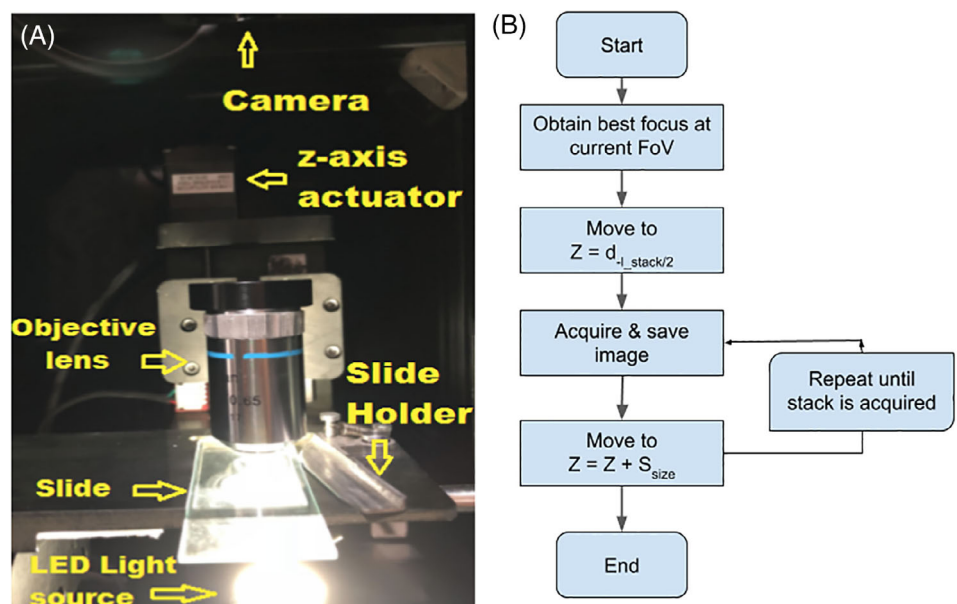


**FIGURE 1** A, Photograph of the imaging section in the setup used for acquiring human blood and PAP smear microscopy images, B, flowchart of the major steps involved in focal stack acquisition

significantly [12]. Further, since the method optimizes the contrast, there is no one-to-one relationship between the pixel values of the original and the enhanced image. Hence, the CLAHE enhanced images are not suitable for quantitative measurements which depend on the physical meaning of the image intensity [12].

### 2.3 | Reduced reference image quality metric for contrast change-based optimal histogram matching for automatic enhancement

An alternative approach to enhancing the contrast of microscopy images is to frame it as an optimization problem. However, this methodology requires tuning of the parameters to result in best output; thus, there is a need for devising an automatic method for contrast enhancement. Such a method has been proposed [13] using a quality metric called as Reduced-reference Image Quality Metric for Contrast Change (RIQMC). This correlates the human visual perception to image contrast as the target image. The same work has further proposed an automatic contrast enhancement based approach, reference optimal histogram matching (ROHIM) based on RIQMC. Images having better visual quality and better contrast can be generated by using a compound function that consists of mean shifting followed by logistic transfer. The contrast enhancement procedure is a blind process, which does not require any reference image quality assessment metric, and requires short execution time to find the optimal histogram mapping in the optimization function. ROHIM essentially consists of two steps:

- Adjusting the input image histogram based on the compound function.
- Finding the optimal parameter maximizing the target function for calculating RIQMC.

The RIQMC metric consists of fusion of information to integrate the difference of phase congruence based entropy and the fourth order statistics. It has been applied successfully to improve contrast in the natural images [13]. For more details, the readers are encouraged to refer to ref. [13].

### 2.4 | Modified $L_0$ based enhancement

Automatic enhancement of contrast is time consuming and computationally demanding. This can be aided by local filters which have a low computational complexity, but they suffer from halos near the edge. These can be

overcome by using global optimization filters. In ref. [19], a  $L_0$  norm based algorithm was proposed, which was used to fuse images having different exposure [19], and art-photographic detail enhancement [20]. The disadvantage of  $L_0$  based algorithm is that it suffers from reversal halos near edges. In ref. [21], a model was proposed which can solve this problem, though with a large computational overhead. Therefore, a new modified  $L_0$  based algorithm, that can amplify the fine details by enlarging the gradients of the source image without disturbing the pixels at the edges was proposed in ref. [14]. The optimization problem consists of a data fidelity term and a regularization term, given by

$$\min_{x_E} \left\{ \sum_p (x_E^p - x_O^p)^2 + \lambda \cdot C(x_E - K \circ x_O) \right\} \quad (1)$$

where,  $x_E$  represents the enhanced image,  $x_O$  represents the OoF input image,  $p$  is the pixel index of the image,  $\circ$  denotes the element-wise product operator and  $\lambda$  is the Lagrangian factor which is used to control the degree of enhancement. Here,  $C(x_E - K \circ x_O)$  is the  $L_0$  norm of the gradient field which equals the number of nonzero elements of the gradient field, and  $K_p$  is defined as

$$K_p = 1 + \frac{k}{1 + e^{\eta \cdot (V_p - \bar{V}_p)}} \quad (2)$$

where,  $k$  denotes the detail layer enhancement,  $V_p$  is the variance of the pixels in the  $3 \times 3$  neighborhood of the  $p^{th}$  pixel,  $\bar{V}_p$  is the mean value of all the local variances and  $\eta$  is calculated as  $\ln(0.01) / (\min(V_p) - \bar{V}_p)$ . In the experiments conducted in this work, the value of  $\lambda$  was set to 0.16 and  $k$  was set to 4. Note that this method has been successfully deployed for enhancement of natural images.

### 2.5 | MV bitonic filter based enhancement

A bitonic sequence is one which monotonically increases to the maximum value and then monotonically decreases, that is, it has atmost one local maxima. Alternatively a signal can be said to be bitonic, if it has either only one local maxima, or only one local minima, or no maxima or minima [22].

The concept of bitonicity is associated with the ordering of the data instead of the actual value and hence the concept of rank filters or order-statistic filters was utilized for the purpose. A rank filter is a generalization of the median filter where any centile can form the output and

thus creating different filters based on the different centile. These filters are monotonic in sense that they preserve signals which are monotonically increasing or decreasing leading to reduction in the impulsive noise as the impulses are bitonic rather than monotonic. Similarly for a two-dimensional (2D) data or image, the shape of the window used to form the set of ranked data is known as the “structuring element” which defines the features preserved after the filtering operation. In case of bitonic filter a circular disk was deployed as mask for 2D image data to ensure isotropic behavior [23].

The Bitonic filtering uses only circular masks which can be further improved by introducing masks of other shapes and hence the performance of the filter can be improved. This concept of using structurally varying masks has been a subject of research and recently, structurally varying bitonic filter with multi-resolution was introduced showing an improvement over the performance of the bitonic filter. The spatial mask utilized for processing of images is typically circular. As structure varies, the MV Bitonic filter adapts the mask without following the patterns in the noise. MV Bitonic filter uses robust structurally varying morphological operations and a novel formulation of Gaussian filtering. For a detailed explanation, the readers may refer to the ref. [15]. This filter was combined with the multi-resolution steps and the noise threshold is added and named as MV Bitonic filters. The main steps of the filter are as follows:

- The mask radius an initial centile are set to a threshold level of 4%. The details of how to set the mask set and centile are given in ref. [15].
- The degree of anisotropy and the local direction for the desired filtering are calculated for the grayscale image or the gray scale version of the colored image. The optimal set of mask shapes and the orientation is calculated using trialing.
- The degree of anisotropy and the local direction are updated using the values of optimal masks and the orientation.
- Perform the structurally varying opening and closing operations on each image channel.
- The optimal set of masks and the orientation is used to improve the degree of anisotropy and the local direction.
- The smoothed errors for each channel and the anisotropy and orientations are calculated.
- The smoothed errors are combined with the structurally varying opening and closing with  $m = 3$ .

## 2.6 | Unsharp mask filter based enhancement

Unsharp masking is a process where an image is sharpened by subtracting a blurred (unsharp) version of the image from the original image. It is being used by the publishing and the printing industry for a number of years [16]. It falls in the class of bilateral filters, which are known to be providing denoised images with preservation of edges. Please refer to ref. [16] for more details about the filter. It consists of the following steps:

- Blur the original image using a Gaussian kernel
- Create a mask which is the difference of the blurred image from the original image.
- Final image is the sum of the mask and the original image.

It consists of two parameters to control the blur and the weight of the filter:

- Radius: It is the standard deviation of the Gaussian blur which is to be subtracted
- Mask Weight: It determines the strength of the filtering

It emphasizes the change in slope of the intensity and can also create negative values, if the actual image contains zero values. These negative values can lead to a halo around the edges [16]. The unsharp masking is an effective method for enhancing a low contrast images. As it does not have regularization built into it, even the noise gets enhanced along with feature information, and it may lead to poor visual perception [24, 25].

## 2.7 | Joint bilateral filter based enhancement

Bilateral filter is a spatial filter proposed initially for performing denoising, detail transfer, sharpening, detail enhancement as well as contrast management. The basic bilateral filter usually causes either over-blur or under-blur in the image features. Therefore, a joint bilateral filter was utilized here for better estimation of the high frequency information from the image [17, 26]. A general linear translation variant filtering process involves the input image ( $x_O$ ), the guidance image ( $x_I$ ) (same as the input image for enhancement) as well as the output image ( $x_F$ ). The filtering at any pixel is given as:

$$x_F = \sum_j W_{ij}(x_I)x_O \quad (3)$$

here,  $i$  and  $j$  represents the pixel indices. The filter kernel  $W_{ij}$  is a function of only the guidance image and does not depend on the input image. The bilateral filter kernel  $W_{ij}^{bf}$  is given as:

$$W_{ij}^{bf}(x_I) = \frac{1}{M_i} \exp\left(-\frac{\|\mathbf{p}_i - \mathbf{p}_j\|^2}{\sigma_s^2}\right) \exp\left(-\frac{\|x_{I_i} - x_{I_j}\|^2}{\sigma_r^2}\right) \quad (4)$$

here,  $\mathbf{p}$  denotes the pixel coordinates and  $M_i$  denotes the normalizing parameter such that  $\sum_j W_{ij}^{bf} = 1$ . The parameter  $\sigma_s$  adjusts the sensitivity of spatial similarity, while the parameter  $\sigma_r$  adjusts the intensity/color similarity. The enhanced output image thus becomes

$$x_E = c * x_D + x_F \quad (5)$$

where  $x_D = x_O - x_F$  is the detailed image and  $c$  is the required magnification for the detailed image.

The joint bilateral filter is known to be an edge-preserving enhancement filter used in many applications [17]. In here, the structural information from other patches in the image gets utilized for defining a guide weight (as each pixel is replaced by a weighted average of its neighbors) leading to better edge-enhancement as well as noise suppression through robust estimation and is known to be a spatial sharpening algorithm, similar to proposed GFGF.

## 2.8 | Proposed GF based enhancement

Filtering is a well-known technique for enhancing the signal and suppressing the noise in images [27]. Many filters such as Gaussian, Laplacian, Non Local Means (NLM) [28] and so on have been used for deblurring, sharpening and restoration of images [16]. These are spatially invariant and independent of the imaging model. Their performance depends on the additional information provided that can be used in the filtering process. Some of these are computationally inefficient and thus have limited utility in real-time processing requirements.

A recently proposed GF approach uses a fast linear time algorithm and is invariant to the kernel size. The GF is an edge preserving filter which uses a guiding image and performs implicit regularization to enhance the image characteristics. It has established itself as a state-of-the-art method and has found applications in image fusion [11], edge aware smoothing, structure transferring [29], flash/no flash denoising [30], joint upsampling, dehazing [31] and detail enhancement [32]. Previously, GF has been used in photoacoustic imaging

[33] to perform image fusion and enhance the performance of reconstruction algorithms [34]. In this work, GF has been used to enhance the OoF images in the focal stack and the OoF image ( $x_O$ ) itself is used as the guiding image.

Let  $x_O$  denote the OoF image,  $x_F$  the filtered image and  $x_E$  represent the enhanced image. The guided filtering process can be represented as a linear transformation of the initial image  $x_O$  to the filtered image  $x_F$  in a window  $\omega_k$  centered at pixel  $k$  and is given as

$$x_F^i = a_k x_O^i + b_k, \forall i \in \omega_k, \quad (6)$$

where,  $a_k$  and  $b_k$  are linear coefficients and are constant in  $\omega_k$ . This model ensures that  $x_F$  has an edge only where  $x_O$  has an edge, as  $\nabla x_F = a \nabla x_O$ . Suppose  $n^i$  is the amount of noise present in the  $x_O$  image, then the reconstructed image  $x_F$  can be represented as

$$x_F^i = x_O^i - n^i \quad (7)$$

The coefficients ( $a_k$  and  $b_k$ ) are determined by minimizing the cost function obtained after combining Equations (6) and (7) and is written as Equations (8).

$$E(a_k, b_k) = \sum_{i \in \omega_k} \left( (a_k x_O^i + b_k - x_O^i)^2 + \epsilon a_k^2 \right) \quad (8)$$

where  $\epsilon$  is the regularization parameter which penalizes larger values of coefficient  $a_k$ . The coefficients obtained after minimizing Eq. (8) are given as Equations (10) and (11).

$$a_k = \frac{\frac{1}{|\omega|} \sum_{i \in \omega_k} x_O^i x_O^i - \mu_k \bar{x}_O^i}{\sigma_k^2 + \epsilon} \quad (9)$$

$$b_k = \bar{x}_O^k - a_k \mu_k \quad (10)$$

with  $\mu_k$  and  $\sigma_k^2$  being the mean and variance of  $x_O$  respectively in  $\omega_k$ ,  $|\omega|$  is the number of pixels in  $\omega_k$  and  $\bar{x}_O^i = \frac{1}{|\omega|} \sum_{i \in \omega_k} x_O^i$  is the mean of  $x_O$  in  $\omega_k$ . Since a pixel is involved in all overlapping windows,  $x_F$  is computed using an average over all windows and the output thus becomes Equations (10) and (11).

$$x_F^i = \frac{1}{|\omega|} \sum_{p|i \in \omega_k} (a_k x_O^i + b_k) \quad (11)$$

Due to the symmetry,  $\sum_{k|i \in \omega_k} a_k = \sum_{k \in \omega_i} a_k$ , Eq. (11) can be written as

$$x_F^i = \bar{a}_i x_O^i + \bar{b}_i \quad (12)$$

The enhanced output image can be written as

$$x_E = c * x_D + x_F \quad (13)$$

where  $x_D = x_O - x_F$  is the detailed image and  $c$  is the required magnification for the detailed image. The steps of the proposed method are presented in Algorithm 1. The enhanced image ( $x_E$ ) computation in the whole process is performed locally patch wise and the computational time required is comparable to any other standard filtering (like Gaussian filter) approach. This enables real-time image enhancement of microscopy images. In case of GF based enhancement, the edge preserving can be explained as follows. The filtering coefficients are given as  $a_k = \frac{\sigma_k^2}{\sigma_k^2 + \epsilon}$  and  $b_k = (1 - a_k)\mu_k$ . When  $\epsilon > 0$ , two cases arise

- If the OoF image ( $x_O$ ) has high variance in  $\omega_k$ , then  $\sigma_k \gg \epsilon$  which implies  $a_k \approx 1$  and  $b_k \approx 0$ . Thus, for a pixel which is present in a high variance area, its value remains the same, that is,  $x_F = x_O$ .
- If the OoF image ( $x_O$ ) is almost constant in  $\omega_k$ , then  $\sigma_k \ll \epsilon$  which implies  $a_k \approx 0$  and  $b_k \approx \mu_k$ . Thus, for a pixel present in a flat patch area, its value becomes the average of the neighboring pixels.

The GF also performs gradient preserving as it uses a patch-wise model. For the enhancement case (same image is used as self-guiding image),  $a_p < 1$  and  $b_p$  is constant.

Suppose the detail layer is given as  $d = x_O - x_F$  and utilizing  $\partial_x x_F = a_k \partial_x x_O$ , one can write

$$\partial_x d = \partial_x x_O - \partial_x x_F = (1 - a_k) \partial_x x_O \quad (14)$$

which implies that  $\partial_x x_d$  and  $\partial_x x_O$  are always in the same direction and thus the gradient is always preserved.

---

**Algorithm 1** Guided Filter( $x_O$ ,  $r$ ,  $\epsilon$ ) with  $f_a(\cdot)$  representing performing operation 'a' on the arguments.

---

Input Input Output Output  $x_O$  – Out of Focus Image  
 $r$  – Window radius(patch size)  
 $\epsilon$  – Regularization Parameters  
 $x_F$  – Filtered Image

- 1:  $mean_{x_O} = f_{mean}(x_O)$
- 2:  $corr_{x_O} = f_{mean}(x_O * x_O)$ ;
- 3:  $var_{x_O} = corr_{x_O} - mean_{x_O} * mean_{x_O}$ ;

$$4: a = var_{x_O} / (var_{x_O} + \epsilon);$$

$$b = mean_{x_O} - a * mean_{x_O}$$

$$5: mean_a = f_{mean}(a);$$

$$mean_b = f_{mean}(b)$$

$$6: x_F = mean_a * x_O + mean_b$$


---

### 3 | EXPERIMENTS

To demonstrate the efficacy of the proposed GF, several focal stacks were acquired from human blood smear and PAP smear slides. The stacks were processed with all enhancement methods presented here, including GF. Slide smears containing healthy as well as *Plasmodium falciparum* infected RBCs were imaged at  $\times 40$  while PAP smears were imaged at  $\times 20$  magnification. Acquisition of these focal stacks of a hundred frames each was performed by first obtaining best focus at a particular Field of View (FoV). The z-axis was then actuated to a particular distance  $d - l_{stack}/2$  below the plane of best focus. This distance was one half of the length of the focal stack ( $l_{stack}$ ) multiplied by the step size ( $s_{size}$ ).

$$d - l_{stack}/2 = - \frac{l_{stack}}{2} * s_{size} \quad (15)$$

The mechanical system then actuates the z-axis in a number of steps totaling to  $l_{stack}$  in a vertical direction upward from the previous location wherein the separation between steps, that is,  $s_{size}$  is programmed to be  $0.33 \mu m$  for blood smear images in Figures 6 and 7 and  $1.00 \mu m$  for the other four focal stacks used in this work. After each translation, a frame is acquired and saved with sequential naming, resulting in a single focal stack. Since the imaging sequence began with a z-plane containing an OoF image and the distribution of the spacing is symmetric along the z-axis, the best focused image is contained at the center of the focal stack.

The unsharp mask filter was applied to images of malaria infected RBCs for different values of the radius and mask weight. The radius was varied through the values (1, 2, 3, 4, 5, 10) while the mask weight was varied through the values (0.1, 0.3, 0.5, 0.7, 0.9). It was observed that the best results were obtained for Radius = 3 and Mask Weight = 0.7 (results not shown) and for rest of the experiments only these values were utilized. It was observed that this filter merely improves the best focused image and its performance degrades when input images are OoF.

The optimal value of the parameter  $\sigma_s$  which adjusts the sensitivity of spatial similarity was found to be 4, while the parameter  $\sigma_r$  which adjusts the intensity/

color similarity was found to be 0.1, and the value of the detail enhancement parameter ( $c$ ) was chosen to be 5. The parameters used for GF approach were as follows:

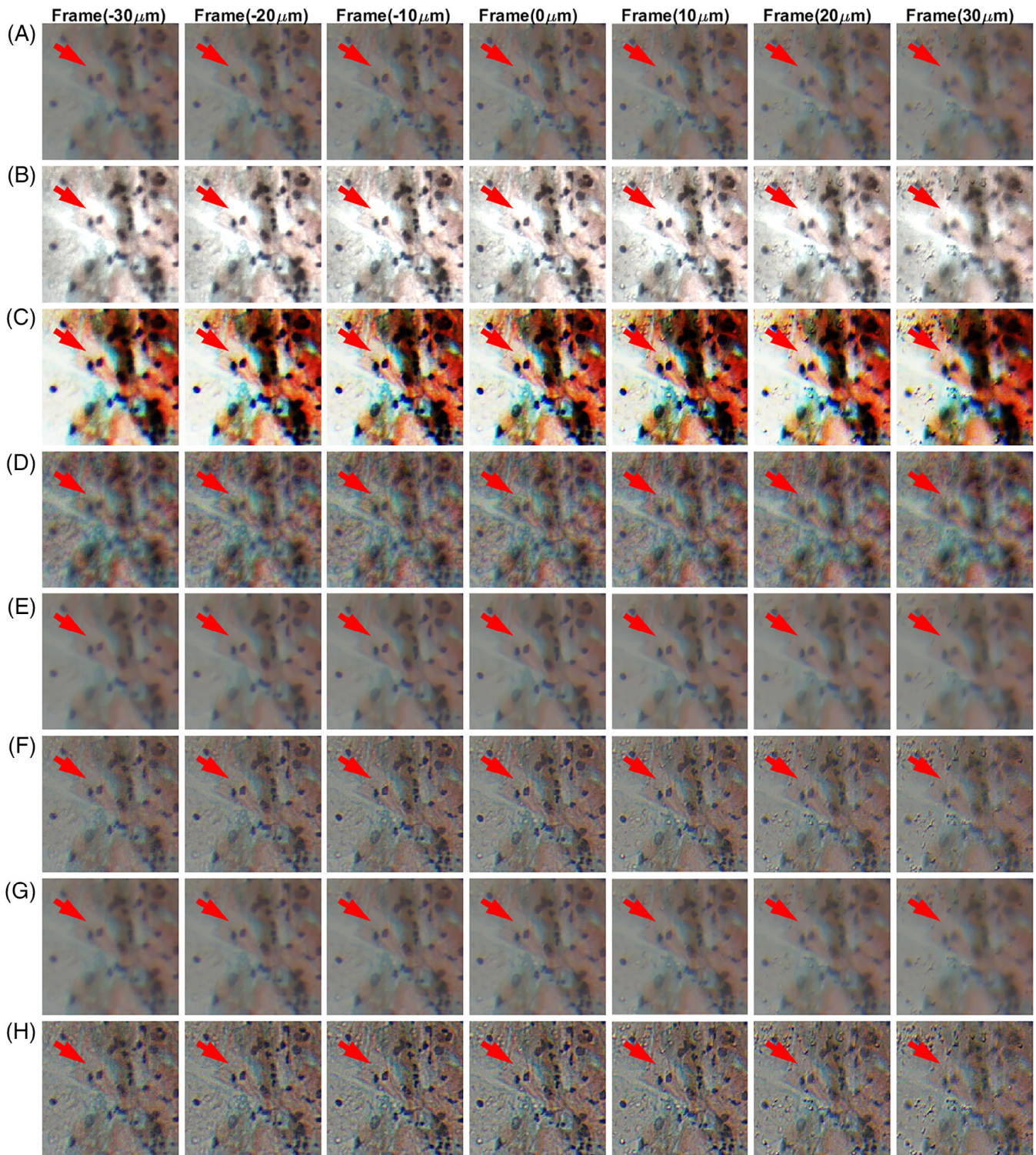


**FIGURE 2** A, The images within a focal stack of PAP smear, after processing with B, CLAHE, C, ROHIM, D, modified  $L_0$ , E, MV-Bitonic, F, unsharp mask filter, G, joint bilateral filter (BF) and H, proposed guided filter (GF). The displayed patch is of size  $320 \text{ px} \times 320 \text{ px}$ . The variance plot for these images is shown in Figure 10. The red arrows indicate one of the enhanced region using the proposed guided filter (g), which was washed off in other enhancement techniques

the patch size defines the neighborhood around the pixel that is used for implicit regularization and the parameter  $\epsilon$  defines the degree of smoothing (defines

the threshold on variance in GF). Here, we have chosen a patch size of 4,  $\epsilon$  as  $1e-2$ , and the value of the detail enhancement parameter ( $c$ ) was chosen to be

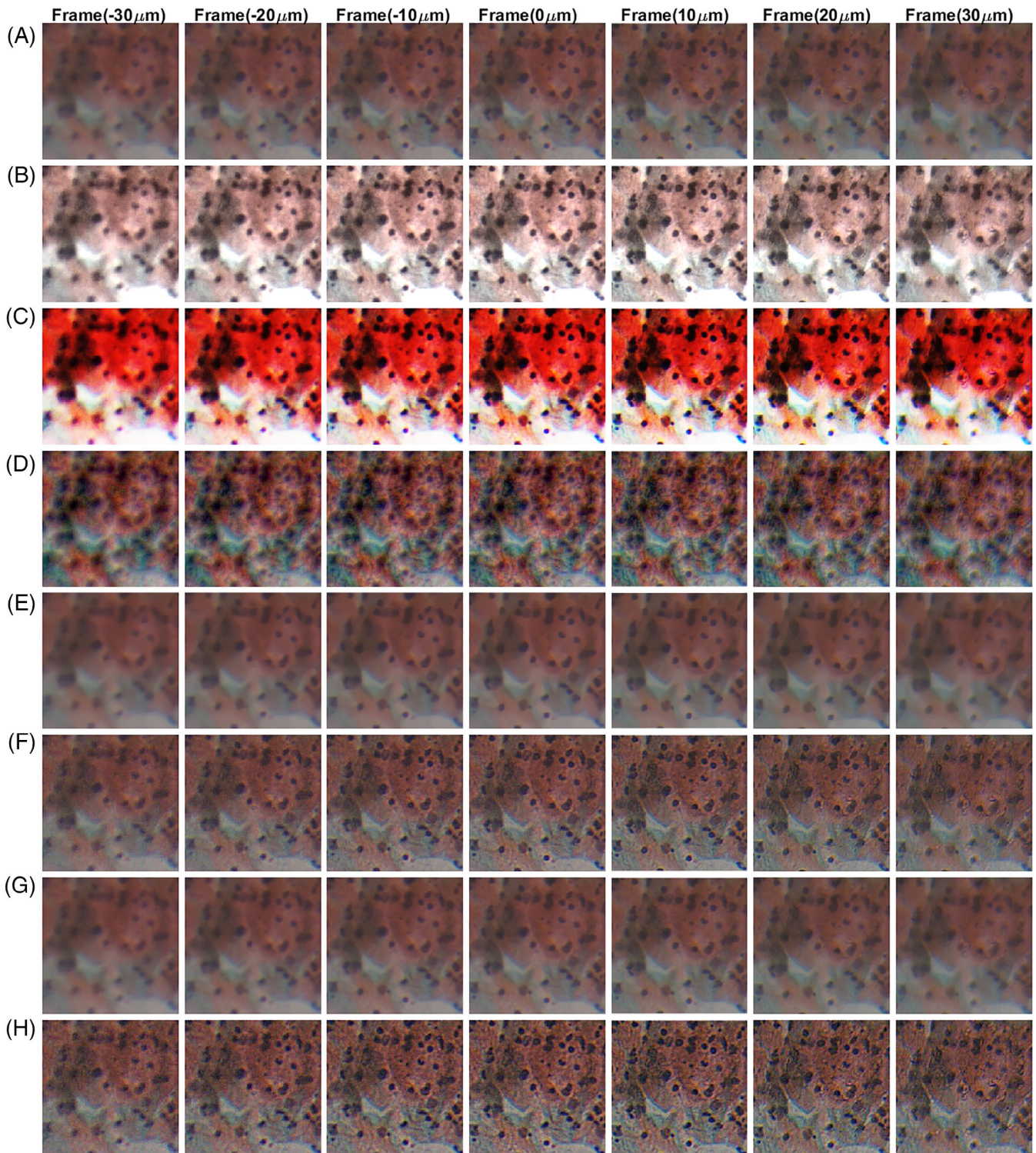


**FIGURE 3** A, The images within a focal stack of PAP smear, after processing with B, CLAHE, C, ROHIM, D, modified  $L_0$ , E, MV-Bitonic, F, unsharp mask filter, G, joint bilateral filter (BF) and H, proposed guided filter (GF). The displayed patch is of size  $320 \text{ px} \times 320 \text{ px}$ . The variance plot for these images is shown in Figure 10

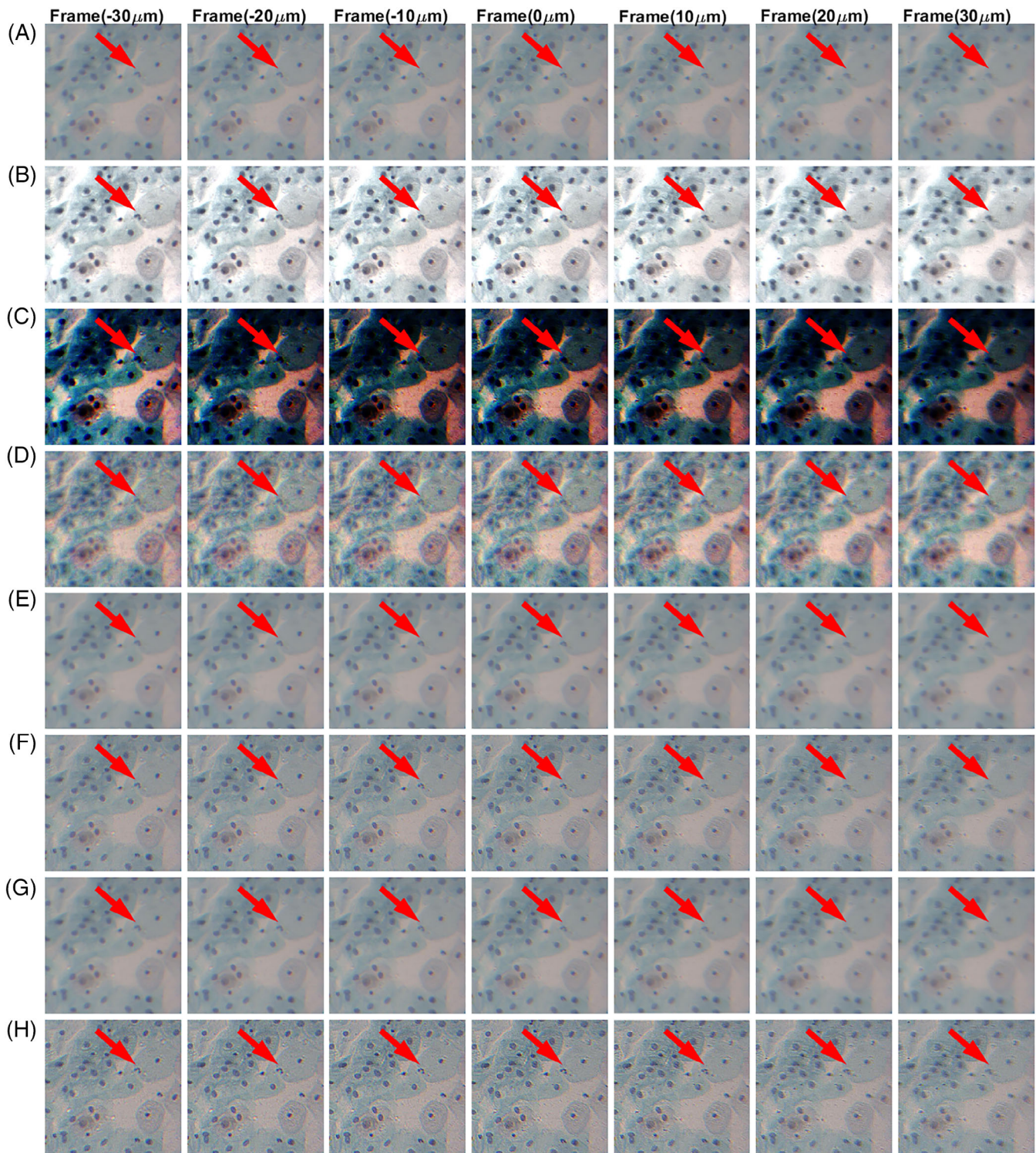


**FIGURE 4** A, The images within a focal stack of PAP smear with epithelial (marked with a red arrow) and nonepithelial cells, after processing with B, CLAHE, C, ROHIM, D, modified  $L_0$ , E, MV-Bitonic, F, unsharp mask filter, G, joint bilateral filter (BF) and H, proposed guided filter (GF). The displayed patch is of size 600 px  $\times$  600 px. The variance plot for these images is shown in Figure 10. The red arrows indicate one of the enhanced region using the proposed guided filter (g), which was washed off in other enhancement techniques

5. For a quantitative measure of the quality of focus, the variance of the image is taken as the method of choice owing to its low computational complexity and appreciable performance.

## 4 | RESULTS AND DISCUSSION

A total of ten set of results are presented here—eight indicating improved visual quality of images (four for PAP smears,

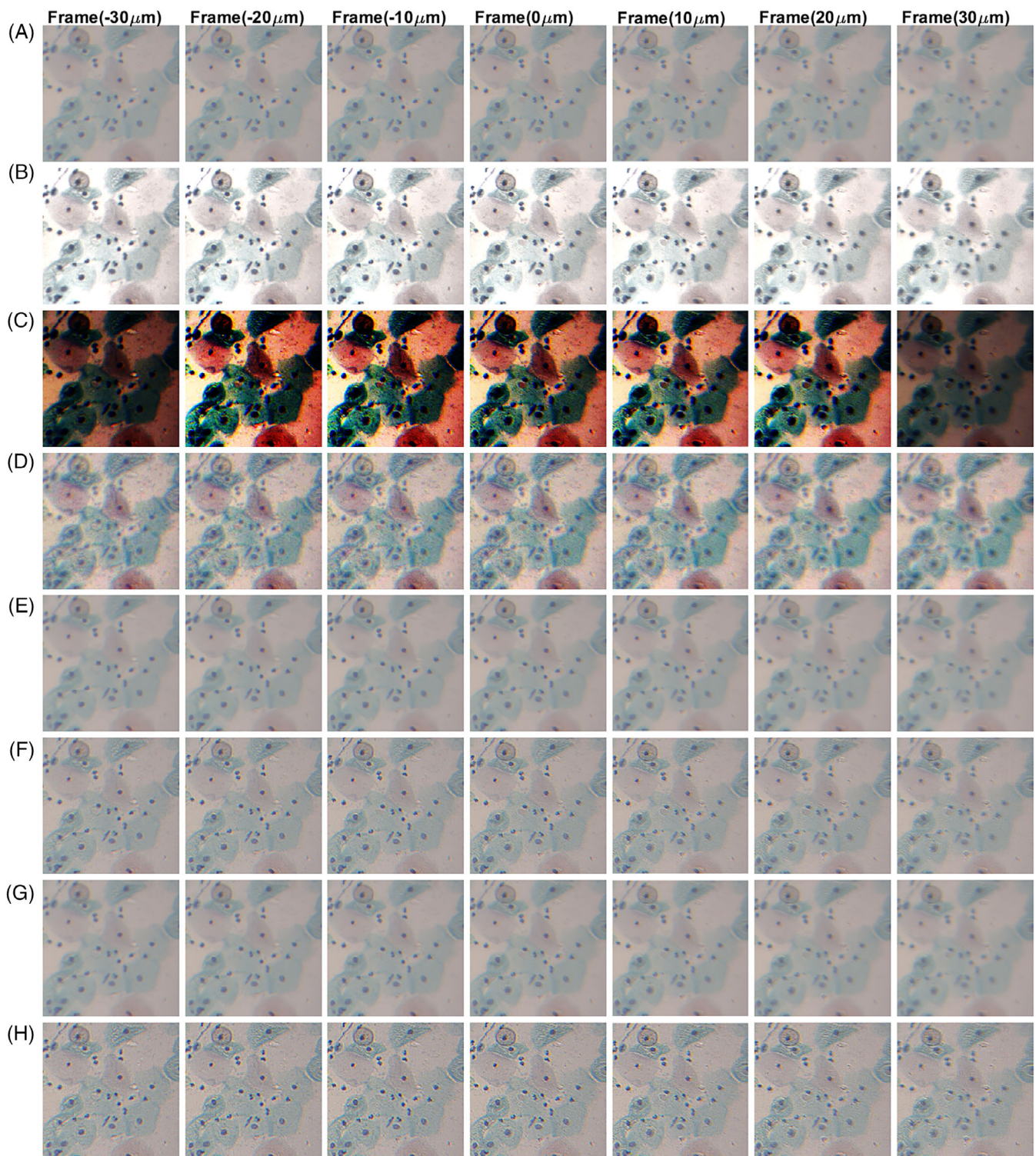


**FIGURE 5** A, The images within a focal stack of PAP smear with epithelial and nonepithelial cells, after processing with B, CLAHE, C, ROHM, D, modified  $L_0$ , E, MV-Bitonic, F, unsharp mask filter, G, joint bilateral filter (BF) and H, proposed guided filter (GF). The displayed patch is of size 600 px  $\times$  600 px. The variance plot for these images is shown in Figure 10

one for a stack of malaria infected RBCs, three for healthy RBCs) and two indicating improved segmentation accuracy (one each for RBC and PAP smear). For all sets, the z-distance from the central frame is shown above each frame.

#### 4.1.1. | Visual quality improvement in PAP smear images

Figures 2 and 3 present few frames from focal stacks of PAP smear slides after enhancement with all six

techniques. Similarly, Figures 4 and 5 present few frames from focal stacks of PAP smear containing epithelial and non-epithelial cells after enhancement with the discussed methods. The optimal performance of GF can be noticed especially in the context of over enhancement, that is, GF preserves the color tone and saturation of image. Both of these are important metrics for histopathology as they can delineate between healthy and abnormal cells when the morphology is otherwise similar. The CLAHE processed images (Figure 2B) appear brighter, but the essential features were absent (indicated via red arrow) in these images when compared to the proposed GF processed images, displayed in Figure 2H, which appear more clear than the native images. ROHIM processed images (Figure 2C) have a different color tone and also cell boundaries were not clear. Lastly, modified  $L_0$  (Figure 2D) and MV-Bitonic (Figure 2E) do not seem to improve the image quality either. While the former produces an undue contrast change without sharpening the features, the latter only serves to smoothen the image, without a significant visual improvement. Here also the maximum distance from the best focused image is greater than  $10\ \mu\text{m}$  and hence the unsharp mask filter (Figure 2F) has limited utility as compared to the GF (Figure 2H). Similar analysis was performed for other focal stacks of PAP smear as shown in Figures 3 to 5. It is evident from these results that other algorithms have limited utility and performs well only for images which are slightly OoF. Once the defocus is more than  $10\ \mu\text{m}$ , their contrast enhancement and image quality improvement is negligible, while the GF provided more promising performance. Similarly, the joint bilateral filter results (Figure 2G), which is another spatial sharpening filter like proposed GF, are also subpar as compared to the image enhancement using GF (Figure 2H).

The variance across each of the focal stacks is presented in Figure 10 (upper left corner image) for all the methods discussed. The GF enhanced images report a higher variance than the native images, indicating a sharper and better focused image. Even though CLAHE provides higher variance, those images lack significant diagnostic information as observed in Figure 2B. The variance is maximum for images processed using ROHIM (Figure 2C), but it over enhances and gives a different color tone to the image. The modified  $L_0$  based method tries to preserve the color tone but the OoF images (shown in Figure 2D) were not improved for the PAP smear data. The MV-Bitonic processed images (shown in Figure 2E) and the joint bilateral filter (shown in Figure 2G) do not report any significant change in the variance values and thus the magnitudes as well as the trends remain nearly the same as the unprocessed images. The unsharp mask filter (Figure 2F)

also gives blurred images and the sharpness is lower as compared to the GF based enhancement. The results obtained using the proposed GF based method improves the image quality of the OoF image as seen in Figure 2H. Unlike the other methods, proposed GF method does not over enhance or change the color tone of the OoF image.

Another benefit of using image GF is that it provides gradient preservation along with edge enhancement as compared to the other methods [10, 11]. This can be clearly seen in the variance plots (Figures 10 and 11) as well as indicated by red arrows in Figures 2, 4 and 6. The proposed GF method enhances the variance and does not change the native trend of the stack as can be seen in the variance plots, the same is not true with other enhancement methods.

#### 4.1 | Visual quality improvement in blood smear images

Figures 6 to 9 present some frames from focal stacks of blood smear slides (including Figure 6 showing malaria-infected RBCs). The processed images show trends that were similar as PAP smear, including change in color tones. This becomes even more important for blood smears, since the color of the nucleus denotes how dense it is and any change in the color tone would affect diagnostic accuracy. Thus, retaining the information of color is critical for diagnosis and only the proposed GF is able to preserve this, while also correcting the defocus. Figure 6A shows the OoF frames for the malaria infected RBCs. The images enhanced using CLAHE are shown in Figure 6B which clearly demonstrates the over enhancement present in images. Figure 6C represents the enhancement using ROHIM which has the effect of changing the color tone itself of the image. Modified  $L_0$  based method preserves the color tone but the image defocus (Figure 6D) was not improved. The MV-Bitonic processed images in Figure 6E and the bilateral filter processed images in Figure 6G show no visually noticeable change apart from a slight deblurring. Figure 6H shows the results of the GF approach which clearly preserves the color tone as well as improves OoF images. In here, the maximum defocus is only  $10\ \mu\text{m}$  and hence the unsharp mask filter gives nearly same performance as the GF although the GF gives sharper images (Figures 6F and 7F). It was found that as the distance is greater than  $8\ \mu\text{m}$  the image quality of the unsharp mask filter starts deteriorating, while the GF still gives superior image quality even for the healthy RBC image stack. Thus, the unsharp mask filter gives good performance only when the acquired images are close to the best focus and thus

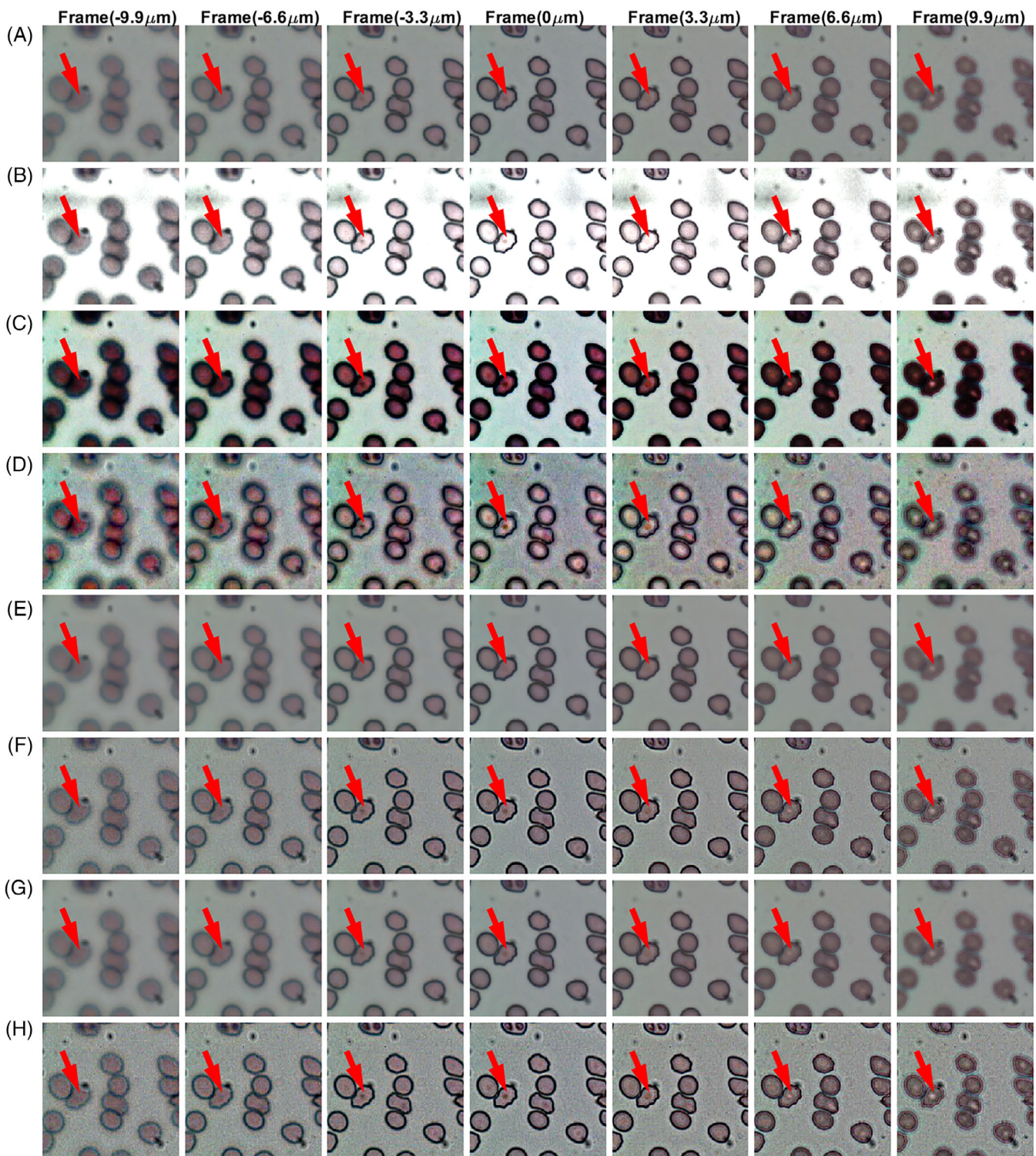


**FIGURE 6** A, The images within a focal stack of malaria (feature marked with red arrow) infected RBCs, after processing with, B, CLAHE, C, ROHIM, D, modified  $L_0$ , E, MV-Bitonic, F, unsharp mask, G, joint bilateral filter (BF) and H, proposed guided filter (GF). The displayed patch is of size 320 px  $\times$  320 px. The variance plot for these images is shown in Figure 11. The red arrows indicate one of the enhanced region using the proposed guided filter (h), which was washed off in other enhancement techniques

will have limited utility in real time. Similar results were obtained for the other focal stacks shown in Figures 7 to 9. The unprocessed stacks are shown in Figures 7A, 8A

and 9A. The over enhanced images using CLAHE are shown in Figures 7B, 8B and 9B, respectively. The images obtained using ROHIM are shown in Figures 7C, 8C and

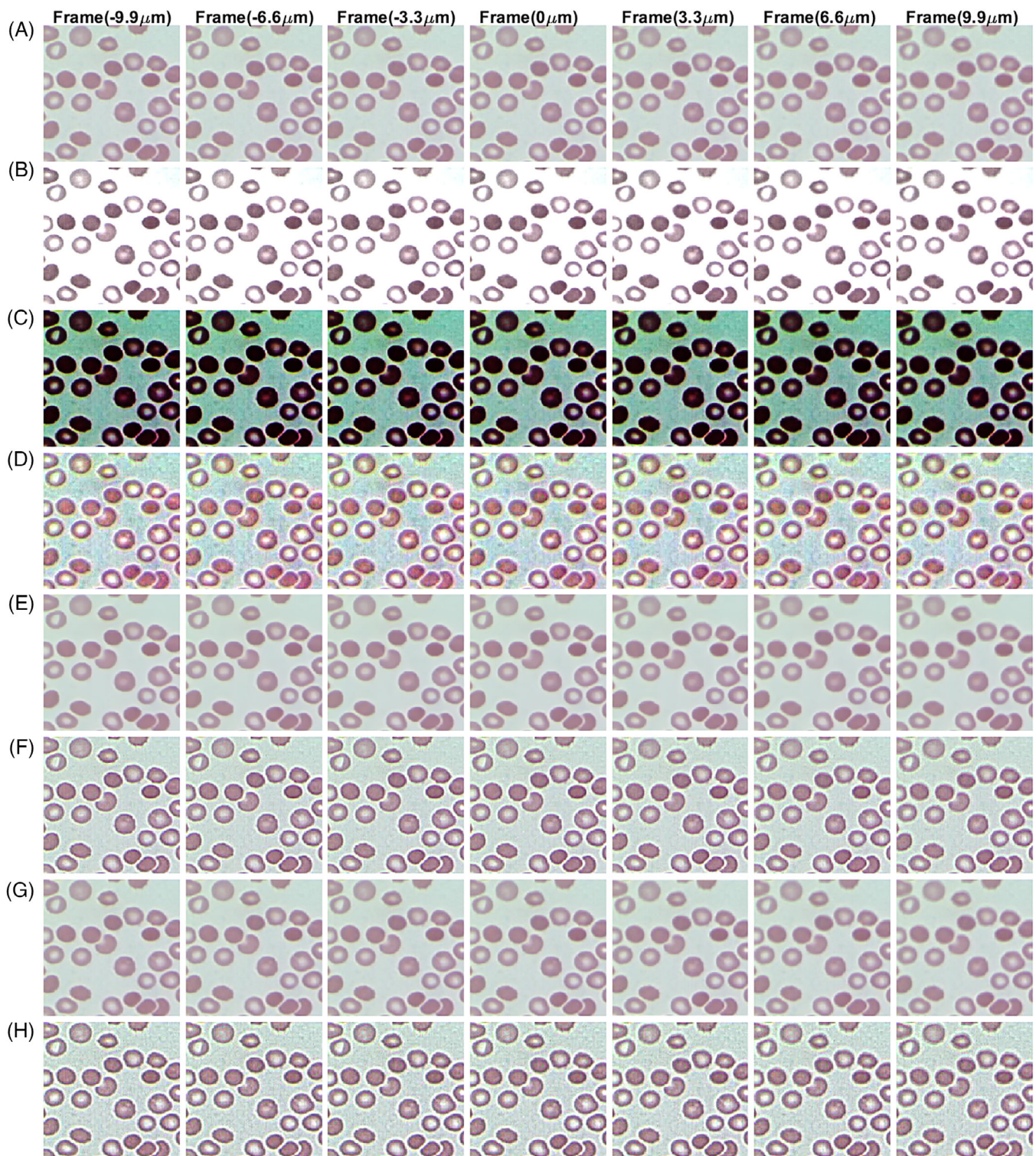


**FIGURE 7** A, The images within a focal stack of healthy RBCs in a blood smear, after processing with B, CLAHE, C, ROHIM, D, modified  $L_0$ , E, MV-Bitonic, F, unsharp mask, G, joint bilateral filter (BF) and H, proposed guided filter (GF). The displayed patch is of size 320 px  $\times$  320 px. The variance plot for these images is shown in Figure 11

9C. The images have a different color tone as compared to input images and defocused images were not improved. Similarly, results obtained using the modified  $L_0$  were represented in Figures 7D, 8D and 9D. These

images show that CLAHE, ROHIM and modified  $L_0$  norm based method do not improve the OoF images. The MV-Bitonic filtered images in Figures 7E, 8E and 9E, results using the unsharp mask filter in

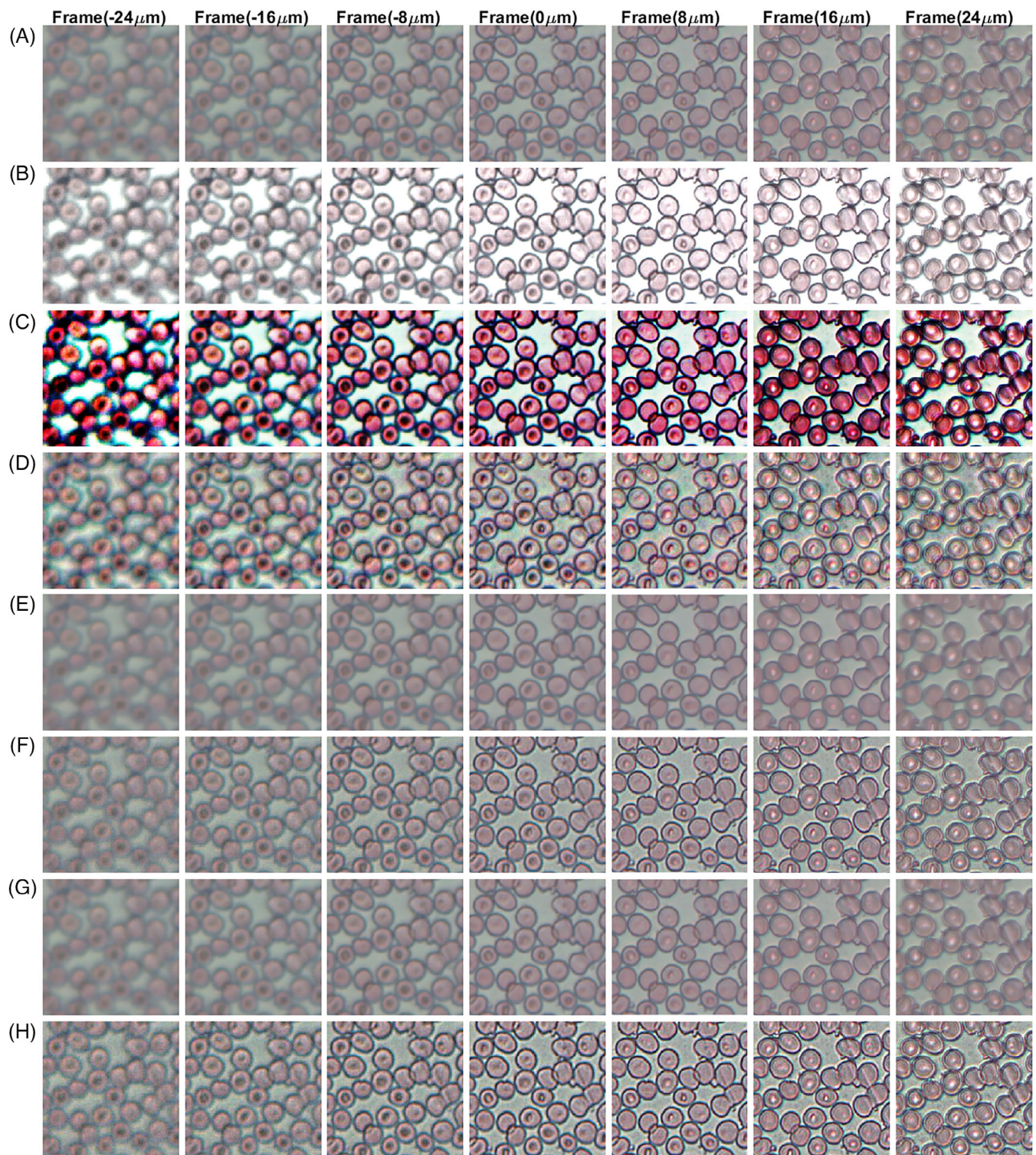


**FIGURE 8** A, The images within a focal stack of healthy RBCs in a blood smear, after processing with B, CLAHE, C, ROHIM, D, modified  $L_0$ , E, MV-Bitonic, F, Unsharp mask, G, joint bilateral filter (BF) and H, proposed guided filter (GF). The displayed patch is of size 320 px  $\times$  320 px. The variance plot for these images is shown in Figure 11

Figures 7F, 8F and 9F and the results using the joint bilateral filter in Figures 7G, 8G and 9G do not demonstrate any useful/significant enhancement. The corresponding processed images for the GF can be seen below each of the focal stacks and the trends

were similar (Figure 11). It must be noted that GF not only preserves cell boundaries (an essential feature in histopathology) and color tone of image, but also significantly improves the clarity of features to the extent that they can be noticed visually (Figures 7H,

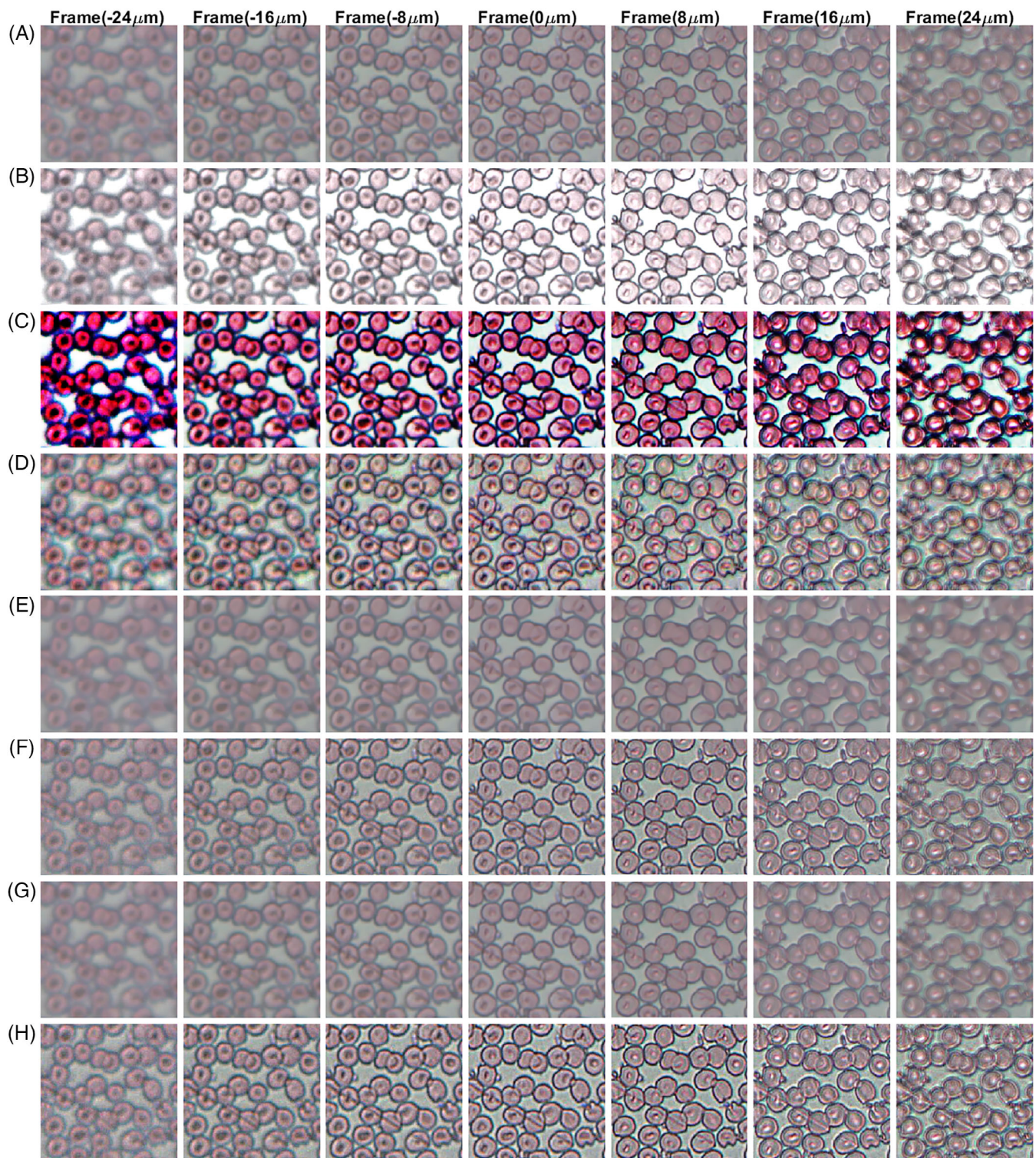


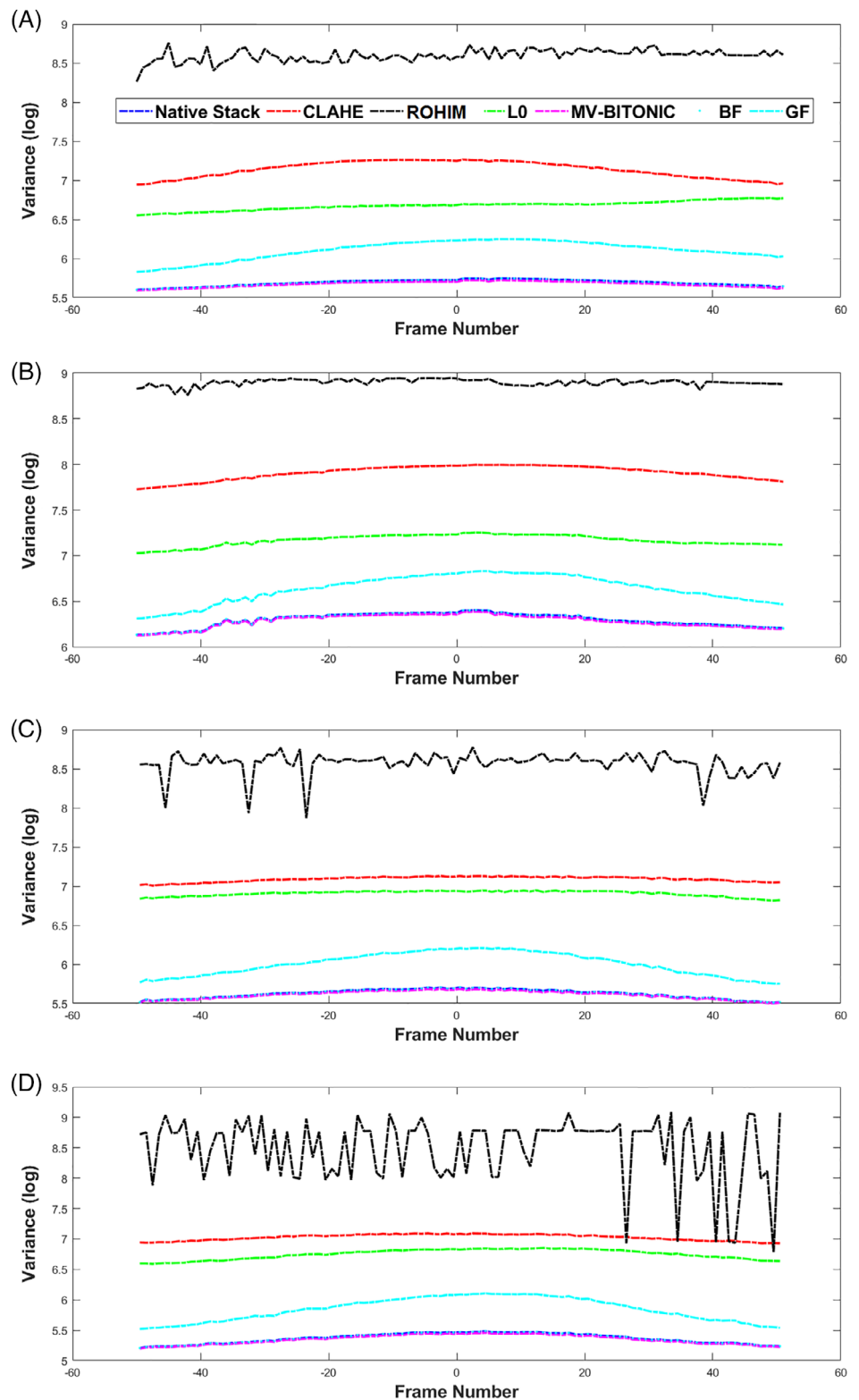
**FIGURE 9** A, The images within a focal stack of healthy RBCs in a blood smear, after processing with B, CLAHE, C, ROHIM, D, modified  $L_0$ , E, MV-Bitonic, F, unsharp mask, G, joint bilateral filter (BF) and H, proposed guided filter (GF). The displayed patch is of size 320 px  $\times$  320 px. The variance plot for these images is shown in Figure 11

8H and 9H). Corresponding plots for variance are shown in Figure 11 for all focal stacks and a major improvement in variance can be seen with the proposed GF.

#### 4.1.1 | Enhancement in segmentation accuracy

To demonstrate the utility of the proposed enhancement, segmentation of the frames containing malaria-infected

**FIGURE 10** The change in variance for the native and enhanced frames of one stack of (Figure 2) PAP smear stack, (Figure 3) another PAP smear stack, (Figure 4) PAP smear stack with epithelial and nonepithelial cells, (Figure 5) PAP smear stack with epithelial and nonepithelial cells. The  $x$ -axis presents the frame number of the corresponding stack while the  $y$ -axis represents the log of the variance



RBCs and PAP smear images was performed after processing the images with all the four methods. The results were compared with those reported by a human expert (a trained personnel with a Master's degree in this field). Five native, OoF frames are shown in Figures 12A and 13A for PAP smear and i-RBC images. Segmentation of these images (Figure 12B) is performed utilizing the

method proposed in ref. [35] which was shown to perform better than CellX segmentation method [37] for i-RBCs. The enhancement was applied using CLAHE, ROHIM and modified  $L_0$ ; subsequently the segmentation was performed and the results were presented in Figure 12C-E. The MV-Bitonic enhanced images are presented in Figure 12F. The unsharp mask enhanced images

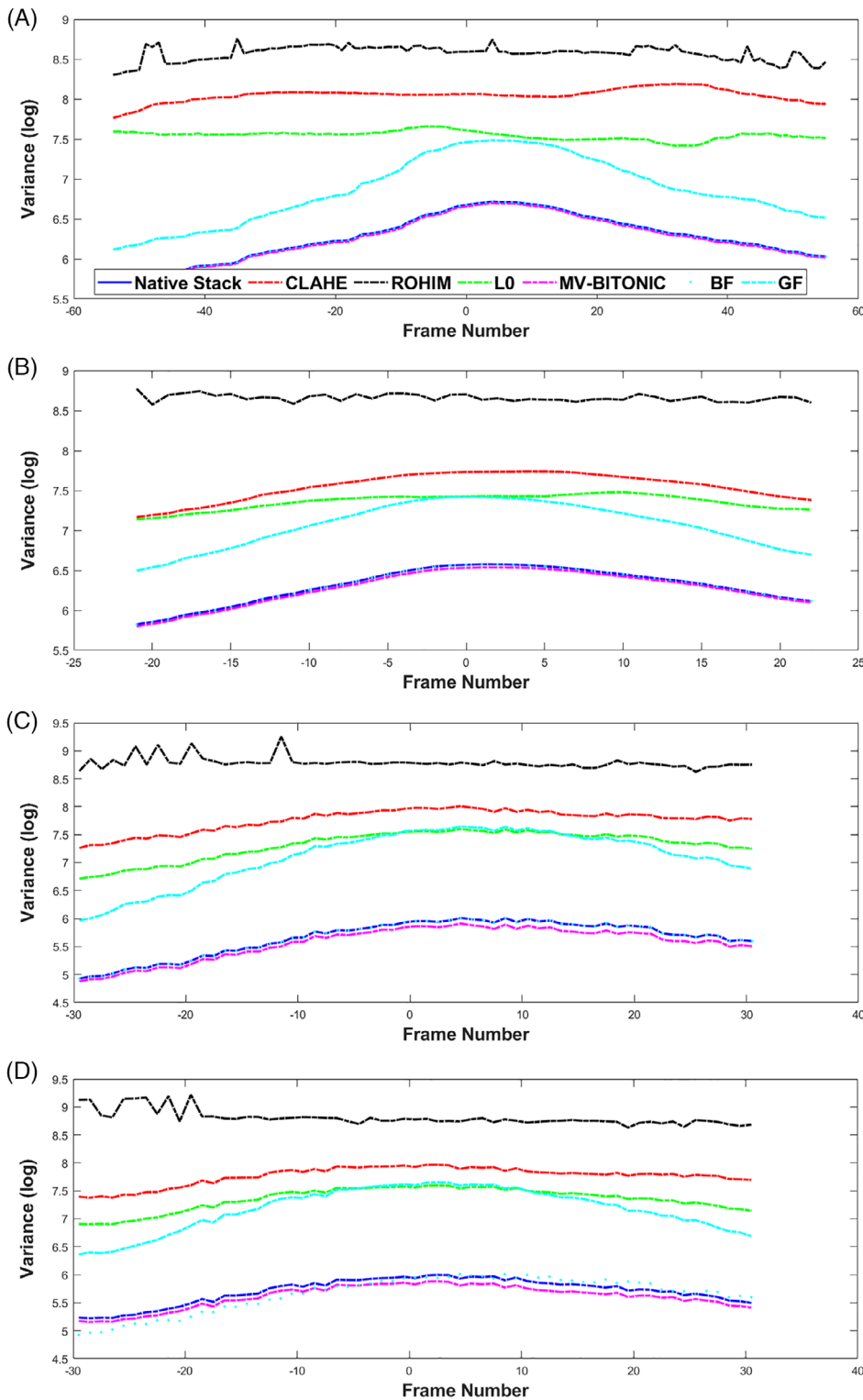
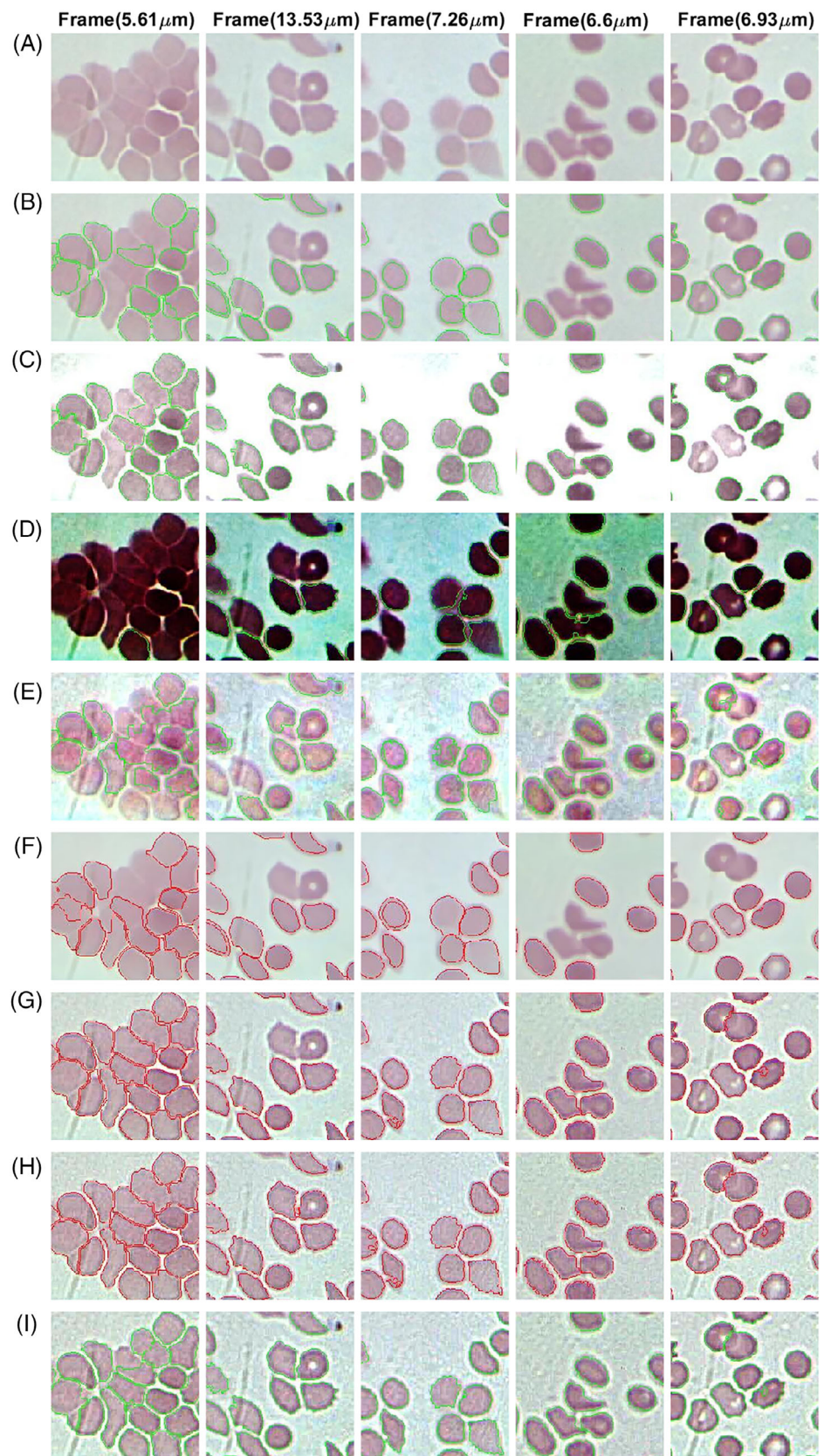


**FIGURE 11** The change in variance for the native and enhanced frames of one stack of (Figure 6) malaria infected RBCs, (Figure 7) healthy RBCs, (Figure 8) another stack of healthy RBCs, and (Figure 9) third stack of healthy RBCs. The x-axis presents the frame number of the corresponding stack while the y-axis represents the log of the variance

are presented in Figure 12G. The joint bilateral filter enhanced images are presented in Figure 12H. The proposed GF was also applied on the native stacks and the improved segmentation results are shown in Figure 12I. Similarly, the segmentation for PAP smear images was performed using the method in ref. [36] for PAP smear images shown in Figure 13A. The results for the

segmentation are shown in Figure 13B for the native stacks. The enhancement was applied using GF on the native stacks and the improved segmentation results are shown in Figure 13I. The segmentation results for other methods were also shown in Figures 13C-H after enhancing images using CLAHE, ROHIM, modified  $L_0$  method, MV-Bitonic, unsharp mask and joint bilateral filter (BF),

**FIGURE 12** A, Five native, OoF frames from different stacks of malaria-infected RBC images, B, their segmentation using the method in [35], the segmentation after processing by C, CLAHE, D, ROHIM, E, modified  $L_0$  method, F, MV-Bitonic, G, unsharp mask, H, joint bilateral filter (BF) and I, proposed guided filter (GF). The displayed patch is of size  $200 \text{ px} \times 200 \text{ px}$ . The segmentation results are given in Table 1. The segmentation contours for cells are overlaid for easy reference



respectively. The MV-Bitonic processed images do show a better segmentation count compared to the native ones. However, it is prone to double/false segmentation

(Figure 12F—column 2 and 3; Figure 13F—column 4) and still does not perform as well as the GF method. After enhancement with GF the features were visible

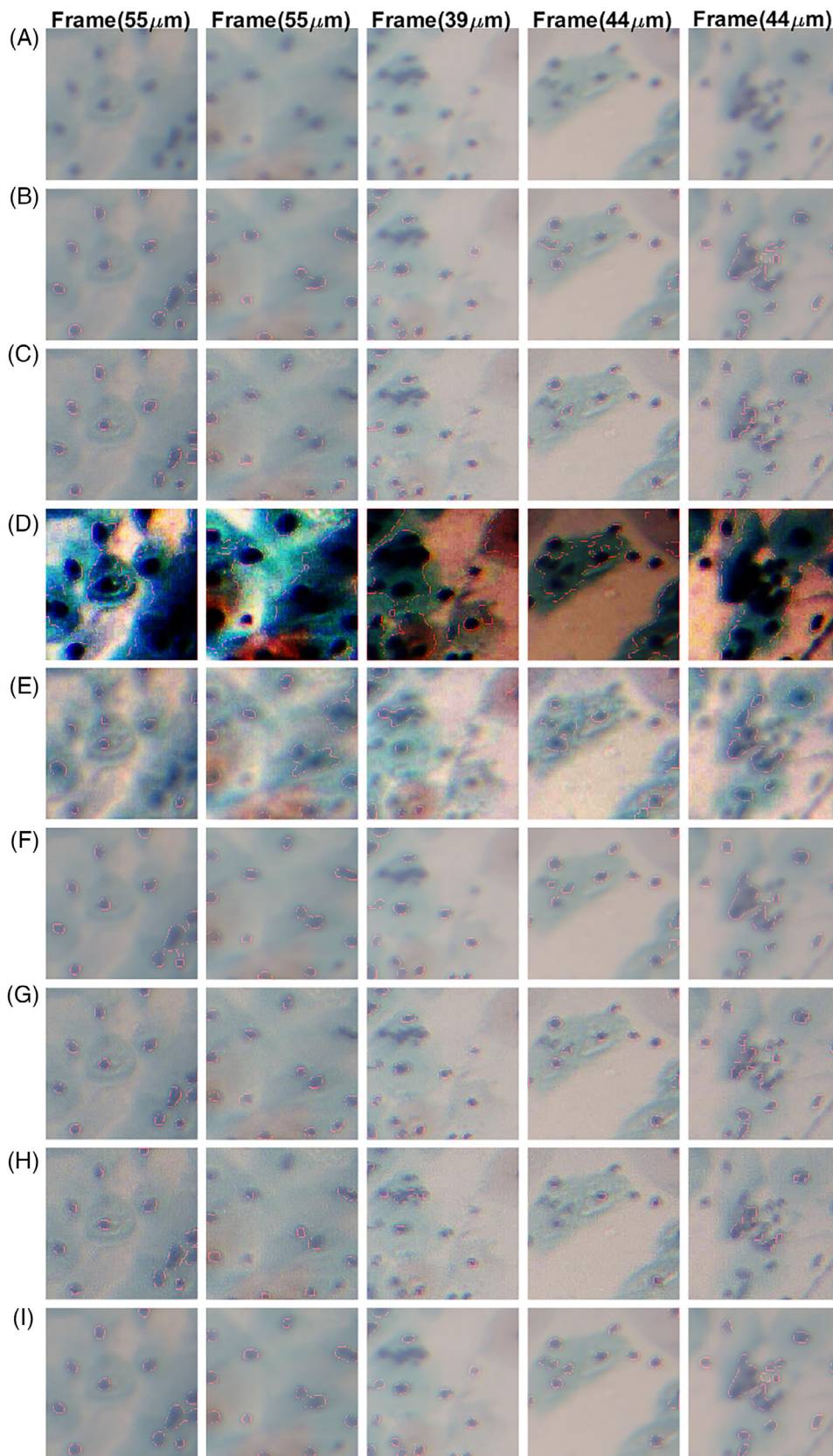


**FIGURE 13** A, Five native, OoF frames from different stacks of PAP smear images, B, segmentation results on native frames using the method in ref. [36], segmentation after processing by C, CLAHE, D, ROHM, E, modified  $L_0$  method, F, MV-Bitonic, G, unsharp mask, H, joint bilateral filter (BF) and I, proposed guided filter (GF). The displayed patch is of size 320 px  $\times$  320 px. The segmentation results are given in Table 1

clearly and it was able to improve the segmentation by 50% for PAP smear and 43% for blood smear, when compared to native images. This resulted in a jump in the

number of cells being identified by the algorithm, as tabulated in Table 1. This improvement is of significant importance since medical professionals rely on the cell

count to arrive at a diagnosis. Even a small improvement of 7% translates to an increase in the RBC count per microliter of blood by 350 000, considering that 1  $\mu$ l blood contains about 5 million RBCs. Such a large increase in accuracy of cell count definitely leads to more accurate diagnosis. It should be noted that GF produces superior images compared to unsharp mask, even if a numerical comparison (on the basis of segmentation results) does not indicate a lot of improvement. Also, as previously discussed that even a small improvement of 7% translates to an increase in the RBC count per microliter of blood by 350 000. GF processed images provides a higher visual clarity than those processed by unsharp mask filter and this is very useful even for a manual diagnosis.

#### 4.1.2 | Computational complexity

All images were taken by a color (RGB) camera at a resolution of 1024 px  $\times$  768 px. The time taken for processing a PAP Smear image is 0.52 seconds for CLAHE, 15.83 seconds for ROHIM, 6.84 seconds for modified  $L_0$ , 212.21 seconds for MV-Bitonic, 0.76 seconds for unsharp mask filtering and 22.3 seconds for joint bilateral filter

while GF takes 0.64 seconds. Note that MATLAB R2019b on a Linux workstation with 16 cores of Intel Xeon processor having a clock rate of 3.0 GHz with 32 GB RAM was used for all computations performed in this work. Such a high-powered system was utilized to achieve low processing times as MATLAB was not optimized for execution speed. The algorithm was intended to be ported to a custom built software using a computationally efficient language such as C, allowing it to be implemented on systems with limited processing power such as cell phones. Further, the algorithm can also be implemented in a dedicated hardware logic using FPGAs, resulting in orders of magnitude reduction in the computational time.

## 5 | CONCLUSION

Automated microscopy and image analysis have the potential to dramatically decrease the turnaround time and increase the reliability of several routinely conducted diagnostic tests. Unfortunately the available commercial equipment for this purpose are too bulky and prohibitively expensive to be deployed in resource constrained settings. While alternate, low-cost designs have been reported in

**TABLE 1** Segmentation results on h-RBC and PAP smear images

<b>Frame number (blood smear) Figure 12</b>	<b>(1)</b>	<b>(2)</b>	<b>(3)</b>	<b>(4)</b>	<b>(5)</b>
<i>RBC present (human expert)</i>	19	16	13	11	17
RBC identified in native image	14	14	13	7	15
RBC identified in CLAHE enhanced image	17	13	13	8	10
RBC identified in ROHIM enhanced image	1	11	13	8	8
RBC identified in Modified $L_0$ enhanced image	10	12	10	9	12
RBC identified in MV-bitonic enhanced image	16	13	12	6	12
RBC identified in unsharp mask enhanced image	19	13	12	10	17
RBC identified in BF enhanced image	19	15	12	10	17
<i>RBC identified in proposed GF enhanced image</i>	19	15	13	10	17
Enhancement using proposed GF over native image	35%	7%	0%	43%	13%
<b>Frame number (PAP smear) Figure 13</b>	<b>(1)</b>	<b>(2)</b>	<b>(3)</b>	<b>(4)</b>	<b>(5)</b>
<i>Cells present (human expert)</i>	12	14	16	13	18
Cells identified in native image	8	11	14	13	11
Cells identified in CLAHE enhanced image	12	14	14	13	11
Cells identified in ROHIM enhanced image	4	7	14	7	7
Cells identified in modified $L_0$ enhanced image	11	10	8	10	7
Cells identified in MV-bitonic enhanced image	11	15	15	12	13
RBC identified in unsharp mask enhanced image	12	15	13	12	15
RBC identified in BF enhanced image	12	11	9	7	7
<i>Cells identified in proposed GF enhanced image</i>	12	15	16	13	15
Enhancement using proposed GF over native image	50%	9%	14%	0%	36%

literature, their mechanical imperfections result in images that are OoF. Such images need enhancement to be suitable for automated processing and this work proposes a method to that end. As evident from the improved segmentation accuracy (as much as 50% improvement for PAP smear and 43% for blood smear) and improved score of the focus metric (variance), significant enhancement in the quality of microscopy images has been demonstrated via proposed GF approach. Importantly, these improvements were achieved without any change in the color tone (unlike other methods), which is a critical parameter for accurate diagnosis. This enhancement eliminates the imperative need of hi-fidelity imaging, which is difficult to achieve in low-cost whole slide imagers. Thus, the cripplingly low throughput caused by acquiring a large focal stack and then selecting the best focused frame at each FoV is eliminated by applying this postprocessing method. Furthermore, the proposed method is very useful whenever a focal stack acquisition is required for imaging thick smears via focal stacking or compensating for substrate surface undulations. In these scenarios, the GF based enhancement can serve to either reduce the number of images required to build the stack or increase the z-separation between the frames, eventually leading to time–cost benefits that are crucial for devices aimed at low-resource settings.

## ACKNOWLEDGMENTS

Phaneendra K. Yalavarthy acknowledges the DST-ICPS cluster funding (T-851) for the data science program. Part of the work is supported through IFTAS-CDS Collaborative Laboratory of Data Science and Engineering.

## CONFLICT OF INTEREST

The authors declare that there are no conflicts of interest related to this article.

## DATA AVAILABILITY STATEMENT

The data that support the findings of this study are available from the corresponding author upon reasonable request.

## ORCID

Phaneendra K. Yalavarthy  <https://orcid.org/0000-0003-4810-352X>

## REFERENCES

- [1] C. Derek, R. I. C. Allen, *Histopathology Specimens: Clinical, Pathological and Laboratory Aspects*, Springer, London, **2017**.
- [2] World Health Organization, Center for Disease Control, *Basic Malaria Microscopy: Tutor's guide*, World Health Organization, Geneva, Switzerland, **2010**.
- [3] L. Pantanowitz, P. N. Valenstein, A. J. Evans, K. J. Kaplan, J. D. Pfeifer, D. C. Wilbur, L. C. Collins, T. J. Colgan, *J. Pathol. Inform.* **2011**, 2, 36.
- [4] F. Ghaznavi, A. Evans, A. Madabhushi, M. Feldman, *Ann. Rev. Pathol.: Mech. Dis.* **2013**, 8, 331.
- [5] N. Farahani, A. V. Parwani, L. Pantanowitz, *Pathol. Lab. Med. Int.* **2015**, 7, 23.
- [6] S. Murali, J. V. Adhikari, V. K. Jagannadh, S. S. Gorthi, *Rev. Sci. Instr.* **2018**, 89(2), 023701.
- [7] H. Fukuda, T. Terasawa, S. Okazaki, *J. Vacuum Sci. Technol. B* **1991**, 9(6), 3113.
- [8] J. Yoon, J.-H. Shin, J.-K. Paik, *Visual Communications and Image Processing*, International Society for Optics and Photonics, Bellingham, Washington, USA, **2001**, p. 819.
- [9] I. De, B. Chanda, B. Chattopadhyay, *Image Vision Comp.* **2006**, 24(12), 1278.
- [10] K. He, J. Sun, X. Tang, *IEEE Trans. Pattern Anal. Mach. Intell.* **2013**, 35, 1397.
- [11] S. Li, X. Kang, H. Jianwen, *IEEE Trans. Image Process.* **2013**, 22(7), 2864.
- [12] Karel Zuiderveld, *Graphics gems*, **1994**, 474.
- [13] G. KGGZ, G. Zhai, W. Lin, M. Liu, *IEEE Trans. Cybern.* **2016**, 46(1), 284.
- [14] F. Kou, W. Chen, Z. Li, C. Wen, *IEEE Signal Process. Lett.* **2015**, 22(2), 211.
- [15] G. Treece, *IEEE Trans. Image Process.* **2019**, 29, 336.
- [16] R. C. Gonzalez, R. E. Woods, S. L. Eddins, *Digital Image Processing Using MATLAB*, Pearson Education India, Chennai, India, **2004**.
- [17] G. Petschnigg, R. Szeliski, M. Agrawala, M. Cohen, H. Hoppe, K. Toyama, *ACM Trans. Graphics (TOG)* **2004**, 23(3), 664.
- [18] R. G. Gavaskar, K. N. Chaudhury, *IEEE Trans. Image Process.* **2018**, 28(2), 779.
- [19] Fei Kou, Zhengguo Li, Changyun Wen, Weihai Chen, in *2013 8th IEEE Conf. Indust. Electron. Appl. (ICIEA)*, IEEE, Melbourne, Australia, **2013**, pp. 1398–1403.
- [20] M. Son, Y. Lee, H. Kang, S. Lee, *Computer Graphics Forum*, Wiley Online Library, **2014**, p. 391.
- [21] L. Xu, C. Lu, Y. Xu, J. Jia, *ACM Trans Graphics* **2011**, 30(6), 1.
- [22] Kenneth E Batchner, in *Proc. Spring Joint Comp. Conf. April 30–May 2, 1968*, New York, United States, **1968**, pp. 307–314.
- [23] G. Heygster, *Comp. Graphics Image Process.* **1982**, 19(2), 148.
- [24] S. Thurnhofer, S. K. Mitra, *IEEE Trans. Image Process.* **1996**, 5(6), 950.
- [25] Rajeev Srivastava, JRP Gupta, Harish Parthasarthy, Subodh Srivastava, in *Int. Conf. Contemporary Comp.*, Springer, Noida, India, **2009**, pp. 8–13.
- [26] Carlo Tomasi, Roberto Manduchi, in *Sixth Int. Conf. Comp. Vision (IEEE Cat. No. 98CH36271)*, IEEE, Bombay, India, **1998**, pp. 839–846.
- [27] C. Solomon, T. Breckon, *Fundamentals of Digital Image Processing: A Practical Approach with Examples in Matlab*, John Wiley & Sons, New York, **2011**.
- [28] Antoni Buades, Bartomeu Coll, J-M Morel, in *2005 IEEE Comp. Soc. Conf. Comp. Vision and Pattern Recogn. (CVPR'05)*, IEEE, San Deigo, CA, **2005**, pp. 60–65.
- [29] Xiaoyong Shen, Chao Zhou, Li Xu, Jiaya Jia, in *Proc. IEEE Int. Conf. Comp. Vision*, IEEE, Santiago, Chile, **2015**, pp. 3406–3414.

- [30] H.-J. Seo, P. Milanfar, *EURASIP J. Adv. Signal Process.* **2012**, 30(18), 1.
- [31] C. Xiao, J. Gan, *Visual Comp.* **2012**, 28(6–8), 713.
- [32] J.-H. Kim, W.-D. Jang, J.-Y. Sim, C.-S. Kim, *J. Visual Commun. Image Represent.* **2013**, 24(3), 410.
- [33] N. Awasthi, S. K. Kalva, M. Pramanik, P. K. Yalavarthy, *J. Biomed. Opt.* **2018**, 23(7), 071204.
- [34] N. Awasthi, S. K. Kalva, M. Pramanik, P. K. Yalavarthy, *J. Biomed. Opt.* **2018**, 23(9), 091413.
- [35] G. P. Gopakumar, M. Swetha, G. S. Siva, G. R. K. S. Subrahmanyam, *J. Biophotonics* **2018**, 11(3), e201700003.
- [36] M Nosrati, Ghassan Hamarneh, in *EEE Int. Symp. Biomed. Imaging*, Beijing, China, **2014**, pp. 1–2.
- [37] S. Dimopoulos, C. E. Mayer, F. Rudolf, J. Stelling, *Bioinformatics* **2014**, 30(18), 2644.

**How to cite this article:** Awasthi N, Katare P, Gorthi SS, Yalavarthy PK. Guided filter based image enhancement for focal error compensation in low cost automated histopathology microscopic system. *J. Biophotonics*. 2020;13:e202000123. <https://doi.org/10.1002/jbio.202000123>